EE

Image Effects of Cylindrical Pipes on Continuous Beams

CPBL Technical Report #96-001

by Christopher K. Allen and Martin Reiser

March 14, 1996

IMAGE EFFECTS OF CYLINDRICAL PIPES ON CONTINUOUS BEAMS[1]

Christopher K. Allen and Martin Reiser
Institute for Plasma Research
University of Maryland
College Park, MD 20742

We analyze the image effects of a cylindrical pipe on continuous beams with elliptical symmetry. Differential equations involving the second order moments of a particle distribution are derived. The self-force components are calculated, including the image forces. From the moment equations, a set of KV type equations are developed which include the image effects of a cylindrical beam pipe. These equations are used to analyze the image effects for FODO channels, sheet beams, and a quadrupole matching section.

1.0 INTRODUCTION

In most accelerator applications a particle beam must propagate through a conducting beam pipe. If the beam dimensions are comparable to the pipe dimensions then the image forces from the pipe will affect the beam dynamics. Usually these are unwanted effects, so by studying such phenomena we hope to develop techniques to minimize their influence. In previous works we have analyzed image effects for axisymmetric bunched beams in cylindrical pipes[1,2]. In this paper we continue the analysis for continuous beams having elliptical symmetry. The primary application of these results would be the analysis of magnetic quadrupole transport systems.

In this report we consider continuous beams centered on the z axis, the axis of propagation, having elliptical symmetry. By elliptical symmetry, we mean that the beam is symmetric across the planes x=0 and y=0. Elliptical symmetry also implies that the charge density of the beam in the transverse directions must be constant along concentric ellipses. We assume the beam pipe to be cylindrical with radius b. We also assume the pipe to be perfectly conducting and, for necessity in constructing the Green's function, we hold it at ground potential (this does not affect the analysis). Figure 1 depicts the example situation of a uniform elliptical distribution in a cylindrical pipe. A transverse cross-section of the beam and beam pipe is shown lying in the xy plane. The beam is centered on the z axis (not shown) corresponding to the point $(x,y) = (0,0)$. The beam has x envelope a_x, and y envelope a_y. Of course, for more general distributions a_x and

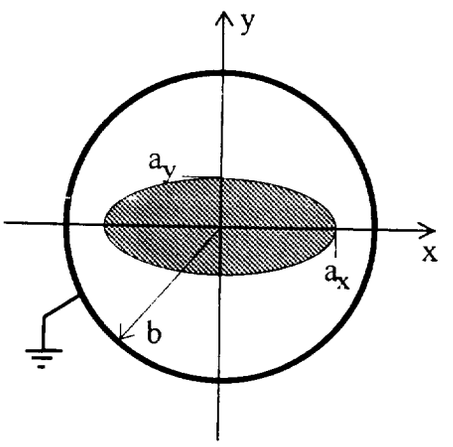

Figure 1: Example geometry of an ellipsoidally symmetric uniform beam in a cylindrical pipe.

[1]Supported by DOE

a_y will no longer be the x and y envelopes of the beam, but will be the major and minor semi-axes of ellipses along which the charge density is constant.

1.1 The Equivalent Beam Concept

Our work is essentially an extension to the results of Sacherer[3]. He derived a set of coupled, ordinary differential equations which describe the evolution of the r.m.s. beam envelope for all continuous beams having elliptical symmetry. These equations have the same functional form as the Kapchinskij-Vladimirskij[4] coupled-envelope equations (KV equations). Indeed, for the uniform distribution these equations are the KV equations exactly. This result leads to the concept of the equivalent KV beam.

Sacherer's formalism allows us to model any continuous beam with elliptical symmetry with an equivalent KV beam. This equivalent beam is a uniform-density, continuous beam having elliptical cross-section and having the same second moments as the actual beam under study. The second spatial moments are also referred to as the r.m.s. envelopes of the beam. The KV equivalent beam has beam envelopes twice that of the actual beams r.m.s. beam envelopes. Also, the emittances of the equivalent beam will be four times the r.m.s. emittances of the actual beam. Thus, the KV coupled-envelope equations may be used to model any continuous beam with elliptical symmetry so long as the r.m.s. beam envelopes and modified emittance values are used in the equation.

The main achievement of our work is the addition of terms to the KV equations which describe the dominant effects of a cylindrical beam pipe. More specifically, we extend Sacherer's equations to include the first-order image effects due to the beam pipe. We then translate these equations to that of the equivalent KV beam. The result is the original KV equations with a term added (to each equation) which accounts for images.

1.2 Limitations and Assumptions

The major shortcoming of this work is the assumption that the r.m.s. beam emittance is either constant or known *a priori*. The forehand knowledge of the r.m.s. emittance through the beam channel is usually an unrealistic expectation. Since r.m.s. emittance growth may occur with nonlinear forces (and the image forces are typically nonlinear), the assumption of a constant emittance leaves us with a potentially inconsistent analysis. Thus, it would seem that the best utilization of our work would be to determine under what conditions image forces play a significant role in the beam dynamics, rather than the precise prediction of beam behavior under the influence of image forces.

In this paper we neglect longitudinal effects. That is we assume that the continuous beam expands and contracts gradually enough to ignore the longitudinal self-fields. Also, this implies that the focusing system is ideal in that no axial forces are produced. With these assumptions we may treat each cross-section of the beam independently. The transverse motion is decoupled from the longitudinal motion and only the transverse self-forces and focusing-forces affect the beam at each cross-section. Thus, for each axial location z we may describe the beam by a distribution function of the transverse phase-space variables x, p_x, y, and p_y.

2.0 MOMENT DIFFERENTIAL EQUATIONS

In this section we develop the differential equations which describe the axial evolution of the particle distribution's second moments. We do so by differentiating the moments of the distribution to yield a set of ordinary differential equations with z as the independent variable.

2.1 Elliptically Symmetric Distributions and Their Moments

Let $n(x,y,p_x,p_y;z)$ be the distribution function for the beam. We let $n(x;y;z)$ denote the marginal distribution function of the configuration coordinates, that is

$$n(x,y;z) \equiv \int_{-\infty}^{+\infty}\int n(x,y,p_x,p_y;z)\,dp_x dp_y . \tag{1}$$

The condition of elliptical symmetry may be expressed by requiring $n(x,y;z)$ to be of the form

$$n(x,y;z) = f\left(\frac{x^2}{a_x^2(z)} + \frac{y^2}{a_y^2(z)}\,;z\right), \tag{2}$$

where $a_x(z)$ and $a_y(z)$ are real, positive-definite functions of z which represent the semi-axes of the concentric ellipses, and f is a positive semi-definite function on the set $[0,\infty)\times\mathbb{R}_+$. Henceforth, for convenience in the analysis we will usually suppress the explicit z dependence in n, f, a_x, and a_y. Note that the above form also implies that the beam is centered on the axis of propagation. Denoting the total number of particles per cross-section as N, we see that

$$\begin{aligned} N &= \int_{-\infty}^{+\infty}\int f\left(\frac{x^2}{a_x^2} + \frac{y^2}{a_y^2}\right) dx\,dy , \\ &= a_x a_y \pi \int_0^{\infty} f(s)\,ds , \end{aligned} \tag{3}$$

where the substitutions $x = a_x r\cos\theta$ and $y = a_y r\sin\theta$ where used to reduce the integral. We note that since we are dealing with a continuous beam N must be constant with respect to z.

We now define the moment operator $\langle\cdot\rangle$ with respect to the distribution n. For an arbitrary function $h(x,y,p_x,p_y;z)$, the moment operator is defined as

$$\langle h\rangle \equiv \frac{1}{N}\int_{-\infty}^{+\infty}\int\int\int h(x,y,p_x,p_y;z)\,n(x,y,p_x,p_y;z)\,dx\,dy\,dp_x dp_y . \tag{4}$$

Note that the moment $\langle h\rangle$ is still a function of the axial coordinate z.

In the Vlasov regime we know that the total time derivative of n is zero (this corresponds to conservation of particle number). Therefore, in a continuous beam where all the particles have the same axial velocity v, we have $d/dt=(d/dz)(dz/dt)$ or $d/dz=(1/v)d/dt$ and we see that the total axial derivative is also zero. This condition allows the operators d/dz and $\langle\cdot\rangle$ to commute. That is $\langle h\rangle'=\langle h'\rangle$ where the prime indicates differentiation with respect to z.

2.2 Equations of Motion

The governing equations for the transverse particle dynamics are Newton's equations. For a particle at the coordinates (x,y) in the xy plane and axial location z, its motion is governed by

$$\begin{aligned} \gamma m\ddot{x} &= F_x(x,y,z), \\ \gamma m\ddot{y} &= F_y(x,y,z), \end{aligned} \tag{5}$$

where the dot indicates differentiation with respect to time, γ is the relativistic factor, m is the particle mass, and F_x and F_y are the forces in the x and y directions, respectively. We assume that transverse velocities are small compared with the longitudinal velocity v so that the total velocity of each particle may be approximated as v. Thus, the relativistic factor γ is approximately constant and given by $1/(1-\beta^2)$ where $\beta=v/c$. We consider a linear focusing system. In this case the forces F_x and F_y have the form

$$\begin{aligned} F_x(x,y,z) &= -k_x(z)x + qE_x(x,y), \\ F_y(x,y,z) &= -k_y(z)y + qE_y(x,y), \end{aligned} \tag{6}$$

where q is the particle charge, $k_x(z)$ represents the external focusing force in the x direction, and E_x is the electric self-field in the x direction. Analogous definitions exist for the y equation.

We may write differential equations for the moments of the distribution n by differentiating the moments with respect to the axial coordinate z. Since the Vlasov equation allows us to differentiate under the moment integral, we may substitute Newton's equations in for the second derivatives of x and y. Using the above forms for the forces in the x and y directions, we have the following equations for the second moments in the x direction (see Sacherer[3]):

$$\begin{aligned} \langle x^2\rangle' &= 2\langle xp_x\rangle, \\ \langle xp_x\rangle' &= \langle p_x^2\rangle - \frac{k_x(z)}{\gamma m v^2}\langle x^2\rangle + \frac{q}{\gamma m v^2}\langle xE_x\rangle, \\ \langle p_x^2\rangle' &= -\frac{2k_x(z)}{\gamma m v^2}\langle p_x x\rangle + \frac{2q}{\gamma m v^2}\langle p_x E_x\rangle, \end{aligned} \tag{7}$$

where $p_x=x'$ and we have substituted $(1/v)d/dz$ for d/dt in Newton's equations. There exists a similar set of differential equations for the y direction.

There are two unknown terms in the above equations, $\langle xE_x\rangle$ and $\langle p_xE_x\rangle$. The term $\langle xE_x\rangle$ will be the major focus of the rest of this paper. The term $\langle p_xE_x\rangle$ is associated with emittance growth in the beam. We avoid considering it by introducing the r.m.s. beam emittances, $\tilde{\epsilon}_x$ and $\tilde{\epsilon}_y$. These quantities are defined as follows:

$$\begin{aligned} \tilde{\epsilon}_x &\equiv \left[\langle x^2\rangle\langle p_x^2\rangle - \langle xp_x\rangle^2\right]^{1/2} = \left[\langle x^2\rangle\langle x'^2\rangle - \langle xx'\rangle^2\right]^{1/2}, \\ \tilde{\epsilon}_y &\equiv \left[\langle y^2\rangle\langle p_y^2\rangle - \langle yp_y\rangle^2\right]^{1/2} = \left[\langle y^2\rangle\langle y'^2\rangle - \langle yy'\rangle^2\right]^{1/2}. \end{aligned} \tag{8}$$

For systems where all forces are linear, it is known that the r.m.s. emittances are invariant[5]. If there exist nonlinear forces (say in E_x) we simply assume that either $\tilde{\epsilon}_x$ is constant or its variation is known *a priori*. We may eliminate $\langle p_x^2 \rangle$ in Eqs. (7) using the first of Eqs. (8). Equations (7) may then be rewritten as one second-order differential equation. Performing a similar procedure for the y equations yields the following set of differential equations for the second spatial moments:

$$\begin{aligned} \langle x^2 \rangle'' - \frac{[\langle x^2 \rangle']^2}{2\langle x^2 \rangle} + \frac{2k_x(z)}{\gamma m v^2}\langle x^2 \rangle - \frac{2q}{\gamma m v^2}\langle xE_x \rangle - \frac{2\tilde{\epsilon}_x^{\,2}}{\langle x^2 \rangle} = 0, \\ \langle y^2 \rangle'' - \frac{[\langle y^2 \rangle']^2}{2\langle y^2 \rangle} + \frac{2k_y(z)}{\gamma m v^2}\langle y^2 \rangle - \frac{2q}{\gamma m v^2}\langle yE_y \rangle - \frac{2\tilde{\epsilon}_y^{\,2}}{\langle y^2 \rangle} = 0. \end{aligned} \tag{9}$$

3.0 COMPUTATION OF $\langle xE_x \rangle$

The only unknown in the first of Eqs. (9) is the quantity $\langle xE_x \rangle$. Sacherer computed this quantity for the free-space situation[3]. He found the surprisingly simple result

$$\langle xE_x \rangle = \frac{qN}{4\pi\epsilon_0}\frac{a_x}{a_x + a_y} = \frac{qN}{4\pi\epsilon_0}\frac{\langle x^2 \rangle^{1/2}}{\langle x^2 \rangle^{1/2} + \langle y^2 \rangle^{1/2}} \tag{10}$$

Note that the above value is independent of the distribution. Substituting this expression for $\langle xE_x \rangle$ in Eqs. (9) leads to Sacherer's equations for the r.m.s. beam envelopes $\langle x^2 \rangle^{1/2}$ and $\langle y^2 \rangle^{1/2}$. However, we wish to include the effects of images in this model. Therefore, we seek to calculate $\langle xE_x \rangle$ in the presence of a cylindrical pipe.

3.1 Polar Coordinates

We will do the field calculations using a two-dimensional analysis in the xy plane. We will also find it convenient to use the polar coordinates (r,θ). The charge distribution ρ has the following form in polar coordinates:

$$\rho(r,\theta) = qf\left(\frac{x^2}{a_x^2} + \frac{y^2}{a_y^2}\right) = qf\left(r^2 u(\theta)\right), \tag{11}$$

where the function $u(\theta)$ is defined

$$u(\theta) \equiv \frac{\cos^2\theta}{a_x^2} + \frac{\sin^2\theta}{a_y^2}. \tag{12}$$

Since we are interested in the computation of $\langle xE_x \rangle$, we wish to express this value in polar coordinates. We find that

$$E_x(r,\theta) = E_r(r,\theta)\cos\theta - E_\theta(r,\theta)\sin\theta. \tag{13}$$

Therefore,

$$\langle xE_x \rangle = \langle r\cos^2\theta E_r \rangle - \langle r\sin\theta\cos\theta E_\theta \rangle. \tag{14}$$

3.2 Green's Function for Poisson's Equation

Poisson's equation in polar coordinates (r, θ) is written

$$\nabla^2\phi(r,\theta) \equiv \frac{1}{r}\frac{\partial}{\partial r}\left(r\frac{\partial\phi}{\partial r}\right) + \frac{1}{r^2}\frac{\partial^2\phi}{\partial\theta^2} = -\frac{\rho(r,\theta)}{\epsilon_0}, \tag{15}$$

where ϕ is the electrostatic potential. We use the Green's function, denoted $g(r,\theta;r_s,\theta_s)$, to invert this equation. It solves the system

$$\begin{aligned} \nabla^2 g(r,\theta;r_s,\theta_s) &= -\frac{\delta(r-r_s)\delta(\theta-\theta_s)}{\epsilon_0}, \\ g(b,\theta;r_s,\theta_s) &= 0 \qquad \text{for all } \theta,\theta_s\in[0,2\pi),\ r_s\in[0,b], \end{aligned} \tag{16}$$

where $\delta(x)$ represents the Dirac delta function. Note that $g(r,\theta;r_s,\theta_s)$ is the potential at the field point (r,θ) due to the unit source at point (r_s,θ_s) when the beam pipe is held at ground potential. The solution to Eq. (15) may be written

$$\phi(r,\theta) = \int_0^{2\pi}\int_0^{b} g(r,\theta;r_s,\theta_s)\rho(r_s,\theta_s)r_s\,dr_s\,d\theta_s. \tag{17}$$

One representation of the Green's function is obtained by expanding it in terms of a trigonometric series in the θ coordinate. That is

$$g(r,\theta) = \sum_{n=-\infty}^{+\infty} g_n(r)\,e^{in\theta}, \tag{18}$$

where the $g_n(r)$ are the coefficients of the expansion. The solution to Eq. (16) using this expansion is given as[6]

$$g(r,\theta;r_s,\theta_s) = \begin{cases} -\dfrac{1}{2\pi\epsilon_0}\ln\dfrac{r_s}{b} - \dfrac{1}{2\pi\epsilon_0}\displaystyle\sum_{n=1}^{\infty}\frac{\cos n(\theta-\theta_s)}{n}\left(\frac{r_s^{\,n}}{b^n}-\frac{b^n}{r_s^{\,n}}\right)\frac{r^n}{b^n} & \text{for } r<r_s, \\ -\dfrac{1}{2\pi\epsilon_0}\ln\dfrac{r}{b} - \dfrac{1}{2\pi\epsilon_0}\displaystyle\sum_{n=1}^{\infty}\frac{\cos n(\theta-\theta_s)}{n}\left(\frac{r^n}{b^n}-\frac{b^n}{r^n}\right)\frac{r_s^{\,n}}{b^n} & \text{for } r>r_s. \end{cases} \tag{19}$$

3.3 The Self-Fields in a Cylindrical Pipe

The potential of a distribution with elliptical symmetry inside the beam pipe may be written by substituting Eqs. (13) and (19) into Eq. (17). The result is

$$\phi(r,\theta) = -\frac{q}{2\pi\epsilon_0}\int_0^{2\pi}\int_0^{r}\left[\ln\frac{r}{b}+\sum_{n=1}^{\infty}\frac{\cos n(\theta-\theta_s)}{n}\left(\frac{r^n}{b^n}-\frac{b^n}{r^n}\right)\frac{r_s^n}{b^n}\right]f(r_s^2u(\theta_s))r_s\,dr_s\,d\theta_s$$
$$-\frac{q}{2\pi\epsilon_0}\int_0^{2\pi}\int_r^{b}\left[\ln\frac{r_s}{b}+\sum_{n=1}^{\infty}\frac{\cos n(\theta-\theta_s)}{n}\left(\frac{r_s^n}{b^n}-\frac{b^n}{r_s^n}\right)\frac{r^n}{b^n}\right]f(r_s^2u(\theta_s))r_s\,dr_s\,d\theta_s. \quad (20)$$

Note how the domains of definition for $g(r,\theta;r_s,\theta_s)$ affect the limits of integration over the r coordinate. Using the relation $\boldsymbol{E}=-\nabla\phi$ where $\boldsymbol{E}$ is the electric field vector, we may compute the two electric field components from Eq. (19) as

$$E_r(r,\theta) = \frac{q}{2\pi\epsilon_0}\int_0^{2\pi}\int_0^{r}\left[\frac{1}{r}+\sum_{n=1}^{\infty}\cos n(\theta-\theta_s)\left(\frac{r^{n-1}}{b^n}+\frac{b^n}{r^{n+1}}\right)\frac{r_s^n}{b^n}\right]f(r_s^2u(\theta_s))r_s\,dr_s\,d\theta_s$$
$$+\frac{q}{2\pi\epsilon_0}\int_0^{2\pi}\int_r^{b}\left[\sum_{n=1}^{\infty}\cos n(\theta-\theta_s)\left(\frac{r_s^n}{b^n}-\frac{b^n}{r_s^n}\right)\frac{r^{n-1}}{b^n}\right]f(r_s^2u(\theta_s))r_s\,dr_s\,d\theta_s, \quad (21)$$

and

$$E_\theta(r,\theta) = -\frac{q}{2\pi\epsilon_0}\int_0^{2\pi}\int_0^{r}\left[\sum_{n=1}^{\infty}\sin n(\theta-\theta_s)\left(\frac{r^{n-1}}{b^n}-\frac{b^n}{r^{n+1}}\right)\frac{r_s^n}{b^n}\right]f(r_s^2u(\theta_s))r\,dr_s\,d\theta_s$$
$$-\frac{q}{2\pi\epsilon_0}\int_0^{2\pi}\int_r^{b}\left[\sum_{n=1}^{\infty}\sin n(\theta-\theta_s)\left(\frac{r_s^n}{b^n}-\frac{b^n}{r_s^n}\right)\frac{r^{n-1}}{b^n}\right]f(r_s^2u(\theta_s))r_s\,dr_s\,d\theta_s, \quad (22)$$

3.4 Computing $\langle xE_x\rangle$

We compute $\langle xE_x\rangle$ in parts according to Eq. (14). We first compute $\langle r\cos^2\theta E_r\rangle$. From Eq. (21) we have

$$\langle r\cos^2\theta\,E_r\rangle = \frac{1}{N}\int_0^{2\pi}\int_0^{b} r\cos^2\theta\,E_r(r,\theta)f(r^2u(\theta))r\,dr\,d\theta$$
$$= \frac{q}{2\pi\epsilon_0 N}\int_0^{2\pi}\int_0^{b}\int_0^{r} rf(r^2u(\theta))\cos^2\theta\left[1+\sum_{n=1}^{\infty}\cos n(\theta-\theta_s)\left(\frac{r^n}{b^n}+\frac{b^n}{r^n}\right)\frac{r_s^n}{b^n}\right]f(r_s^2u(\theta_s))r_s\,dr_s\,dr\,d\theta_s\,d\theta$$
$$+\frac{q}{2\pi\epsilon_0 N}\int_0^{2\pi}\int_0^{b}\int_r^{b} rf(r^2u(\theta))\cos^2\theta\left[\sum_{n=1}^{\infty}\cos n(\theta-\theta_s)\left(\frac{r_s^n}{b^n}-\frac{b^n}{r_s^n}\right)\frac{r^n}{b^n}\right]f(r_s^2u(\theta_s))r_s\,dr_s\,dr\,d\theta_s\,d\theta, \quad (23)$$

where the order of integration between r and θ_s has been interchanged. Note that the r_s integration over the terms containing $(rr_s/b^2)^n$ can be combined to yield an integration over the full interval $[0,b]$. Also, it is possible to further simplify this expression somewhat by changing the order of integration in the second integral (after removing the term containing $(rr_s/b^2)^n$ in the integrand). Figure 2 shows the region of integration in r_s-r space for the second integral. By integrating over r first then r_s we get a region of integration similar to the first integral term. We also switch the order of integration between θ_s and θ to obtain (after relabeling)

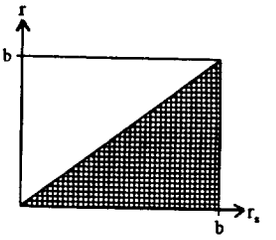

Figure 2: Integration region in r_s-r space.

$$\begin{aligned}\langle r\cos^2\theta\, E_r\rangle &= \frac{q}{2\pi\epsilon_0 N}\int_0^{2\pi}\int_0^b\int_0^r rf(r^2u(\theta))\cos^2\theta f(r_s^2u(\theta_s))r_s\,dr_s\,dr\,d\theta_s\,d\theta \\ &+ \sum_{n=1}^{\infty}\frac{q}{2\pi\epsilon_0 N}\int_0^{2\pi}\int_0^b\int_0^r rf(r^2u(\theta))\left[\cos^2\theta-\cos^2\theta_s\right]\cos n(\theta-\theta_s)\frac{r_s^n}{r^n}f(r_s^2u(\theta_s))r_s\,dr_s\,dr\,d\theta_s\,d\theta \\ &+ \sum_{n=1}^{\infty}\frac{q}{2\pi\epsilon_0 N}\int_0^{2\pi}\int_0^b\int_0^b rf(r^2u(\theta))\cos^2\theta\cos n(\theta-\theta_s)\left(\frac{r^n}{b^n}\frac{r_s^n}{b^n}\right)f(r_s^2u(\theta_s))r_s\,dr_s\,dr\,d\theta_s\,d\theta\,,\end{aligned} \tag{24}$$

Performing similar procedures for $\langle r\sin\theta\cos\theta E_\theta\rangle$ we find that

$$\begin{aligned}\langle r\sin\theta\cos\theta\, E_\theta\rangle &= \\ &\sum_{n=1}^{\infty}\frac{q}{2\pi\epsilon_0 N}\int_0^{2\pi}\int_0^b\int_0^r rf(r^2u(\theta))\left[\sin\theta\cos\theta-\sin\theta_s\cos\theta_s\right]\sin n(\theta-\theta_s)\frac{r_s^n}{r^n}f(r_s^2u(\theta_s))r_s\,dr_s\,dr\,d\theta_s\,d\theta \\ &-\sum_{n=1}^{\infty}\frac{q}{2\pi\epsilon_0 N}\int_0^{2\pi}\int_0^b\int_0^b rf(r^2u(\theta))\sin\theta\cos\theta\sin n(\theta-\theta_s)\left(\frac{r^n}{b^n}\frac{r_s^n}{b^n}\right)f(r_s^2u(\theta_s))r_s\,dr_s\,dr\,d\theta_s\,d\theta\,,\end{aligned} \tag{25}$$

From Eq. (14) we know that the value for $\langle xE_x\rangle$ is given by the difference of Eqs. (24) and (25). Fortunately, we do not have to compute most of the two above expressions; we already know them.

In the limit $b\to\infty$, we expect to recover the free-space solution for $\langle xE_x\rangle$. In this limit, all the terms of Eqs. (24) and (25) containing b in the denominator vanish. Consequently, these must be terms representing the image component of $\langle xE_x\rangle$. Thus, it is possible to identify the terms of Eqs. (24) and (25) corresponding to the free-space component and the image component of $\langle xE_x\rangle$, for which we use the superscripts FS and I, respectively. We have for the image component

$$\langle xE_x\rangle^I = \langle r\cos^2\theta\, E_r\rangle^I - \langle r\sin\theta\cos\theta\, E_\theta\rangle^I$$

$$= \sum_{n=1}^{\infty} \frac{q}{2\pi\epsilon_0 N}\int_0^{2\pi}\int_0^b\int_0^b rf(r^2u(\theta))\cos^2\theta\cos n(\theta-\theta_s)\left(\frac{r^n}{b^n}\frac{r_s^n}{b^n}\right) f(r_s^2u(\theta_s))r_s\,dr_s\,dr\,d\theta_s\,d\theta$$

$$+ \sum_{n=1}^{\infty} \frac{q}{2\pi\epsilon_0 N}\int_0^{2\pi}\int_0^b\int_0^b rf(r^2u(\theta))\sin\theta\cos\theta\sin n(\theta-\theta_s)\left(\frac{r^n}{b^n}\frac{r_s^n}{b^n}\right) f(r_s^2u(\theta_s))r_s\,dr_s\,dr\,d\theta_s\,d\theta\,, \tag{26}$$

and for the free-space component

$$\langle xE_x\rangle^{FS} = \langle r\cos^2\theta\, E_r\rangle^{FS} - \langle r\sin\theta\cos\theta\, E_\theta\rangle^{FS}$$

$$= \frac{q}{2\pi\epsilon_0 N}\int_0^{2\pi}\int_0^b\int_0^r rf(r^2u(\theta))\cos^2\theta\, f(r_s^2u(\theta_s))r_s\,dr_s\,dr\,d\theta_s\,d\theta$$

$$+ \sum_{n=1}^{\infty} \frac{q}{2\pi\epsilon_0 N}\int_0^{2\pi}\int_0^b\int_0^r rf(r^2u(\theta))\left[\cos^2\theta - \cos^2\theta_s\right]\cos n(\theta-\theta_s)\frac{r_s^n}{r^n} f(r_s^2u(\theta_s))r_s\,dr_s\,dr\,d\theta_s\,d\theta \tag{27}$$

$$\sum_{n=1}^{\infty} \frac{q}{2\pi\epsilon_0 N}\int_0^{2\pi}\int_0^b\int_0^r rf(r^2u(\theta))\left[\sin\theta\cos\theta - \sin\theta_s\cos\theta_s\right]\sin n(\theta-\theta_s)\frac{r_s^n}{r^n} f(r_s^2u(\theta_s))r_s\,dr_s\,dr\,d\theta_s\,d\theta\,.$$

The integrand of Eq. (27) may be put into closed form to obtain (see Appendix A)

$$\langle xE_x\rangle^{FS} = \frac{q}{2\pi\epsilon_0 N}\int_0^{2\pi}\int_0^b\int_0^r rf(r^2u(\theta))\frac{\left[r\cos\theta - r_s\cos\theta_s\right]^2}{r^2+r_s^2-2rr_s\cos(\theta-\theta_s)} f(r_s^2u(\theta_s))r_s\,dr_s\,dr\,d\theta_s\,d\theta\,,$$

$$= \frac{q}{2\pi\epsilon_0 N}\int_0^{2\pi}\int_0^b\int_0^r rf(r^2u(\theta))\frac{\left[r\cos\theta - r_s\cos\theta_s\right]^2}{\left[r\cos\theta - r_s\cos\theta_s\right]^2+\left[r\sin\theta - r_s\sin\theta_s\right]^2} f(r_s^2u(\theta_s))r_s\,dr_s\,dr\,d\theta_s\,d\theta\,. \tag{28}$$

The above expression must equate to the free-space solution obtained by Sacherer. That is

$$\lim_{b\to\infty}\langle xE_x\rangle = \langle xE_x\rangle^{FS} = \frac{qN}{4\pi\epsilon_0}\frac{a_x}{a_x+a_y}\,. \tag{29}$$

This identity is valid so long as there exists a suitable buffer region between the charge distribution and the pipe wall. Specifically, b and f must be such that the quantity $f[b^2u(\theta)]$ is zero for all θ in the interval 0 to 2π. In general this is a reasonable assumption. Note that since this is essentially Sacherer's result, the above integral also turns out to be independent of the function f. Using the above identity we find that in the presence of the cylindrical pipe

$$\langle xE_x\rangle = \frac{qN}{4\pi\epsilon_0}\frac{a_x}{a_x+a_y} + \frac{q}{2\pi\epsilon_0 N}\sum_{n=1}^{\infty}\frac{1}{b^{2n}} I_n \tag{30}$$

where the quantity I_n is defined by

$$I_n \equiv \int_0^{2\pi}\int_0^{b} rf(r^2u(\theta))\left[\cos^2\theta\cos n(\theta-\theta_s)+\sin\theta\cos\theta\sin n(\theta-\theta_s)\right](r\,r_s)^n f(r_s^2u(\theta))r_s\,dr_s\,dr\,d\theta_s\,d\theta\,,$$

$$= \left[\int_0^{\infty} s^{n/2}f(s)\,ds\right]^2 \int_0^{2\pi}\int_0^{2\pi} \frac{\cos^2\theta\cos n(\theta-\theta_s)+\sin\theta\cos\theta\sin n(\theta-\theta_s)}{u^{n/2+1}(\theta)\;u^{n/2+1}(\theta_s)}\,d\theta_s\,d\theta\,. \tag{31}$$

The above integrations where separated using the substitutions $s=r^2u(\theta)$ and $t=r_s^2u(\theta_s)$. The first two I_n's are readily identified (see Appendix B).

$$I_1 = \left[\frac{1}{2}\int_0^{\infty} s^{1/2}f(s)\,ds\right]^2 \int_0^{2\pi}\int_0^{2\pi} \frac{\cos\theta\cos\theta_s}{u^{3/2}(\theta)\,u^{3/2}(\theta_s)}\,d\theta_s\,d\theta = N^2\langle x\rangle^2 = 0\,, \tag{32}$$

and

$$I_2 = \left[\frac{1}{2}\int_0^{\infty} sf(s)\,ds\right]^2 \int_0^{2\pi}\int_0^{2\pi} \frac{\cos^2\theta\cos^2\theta_s-\cos^2\theta\sin^2\theta_s+2\sin\theta\cos\theta\sin\theta_s\cos\theta_s}{u^2(\theta)\,u^2(\theta_s)}\,d\theta_s\,d\theta\,, \tag{33}$$

$$= N^2\langle x^2\rangle^2 - N^2\langle x^2\rangle\langle y^2\rangle$$

In a similar fashion we find that $I_3=0$. Therefore, the effects due to the cylindrical pipe is given by the following:

$$\langle xE_x\rangle = \frac{qN}{4\pi\epsilon_0}\left[\frac{\langle x^2\rangle^{1/2}}{\langle x^2\rangle^{1/2}+\langle y^2\rangle^{1/2}} + 2\frac{\langle x^2\rangle}{b^4}\left(\langle x^2\rangle-\langle y^2\rangle\right) + O\left(\frac{\langle x^4\rangle^2}{b^8}, \frac{\langle x^4\rangle\langle y^4\rangle}{b^8}, \frac{\langle y^4\rangle^2}{b^8}\right)\right], \tag{34}$$

where $O(\cdot)$ indicates the standard order notation. The first term in the above equation represents the free-space contribution to $\langle xE_x\rangle$, while the second term represents the contribution due to the charge distribution's quadrupole moment. The last term is meant to indicate that the image forces due to the higher order moments of the charge distribution (octupole moments and up) scale as $\langle x^4\rangle^2/b^8$, etc.

4.0 THE KV EQUATIONS WITH IMAGES

We now use the preceding results to modify the KV equations to include the dominant effects from images. We begin by substituting Eq. (34) into the first of Eqs. (9) to obtain the ordinary differential equation

$$\langle x^2\rangle'' - \frac{[\langle x^2\rangle']^2}{2\langle x^2\rangle} + \frac{2k_x(z)}{\gamma mv^2}\langle x^2\rangle - \frac{2\tilde{\epsilon}_x^{\,2}}{\langle x^2\rangle} - \frac{2q}{\gamma mv^2}\frac{qN}{4\pi\epsilon_0}\left[\frac{\langle x^2\rangle^{1/2}}{\langle x^2\rangle^{1/2}+\langle y^2\rangle^{1/2}} + 2\frac{\langle x^2\rangle}{b^4}\left(\langle x^2\rangle-\langle y^2\rangle\right)\right] = 0\,, \tag{35}$$

where we have ignored the higher order effects. There exists a similar equation for the y direction, which is obtained by interchanging the x's and y's in the above equation. This equation may be cleaned up by recognizing a few standard parameters. First, the generalized beam perveance is defined as[7]

$$K \equiv \frac{qI}{2\pi\epsilon_0\gamma mv^3} = \frac{q^2N}{2\pi\epsilon_0\gamma mv^2}, \tag{36}$$

where I is the beam current. Next, it is customary to use the focusing function $\kappa_x(z)$ rather than the force function $k_x(z)$. These two functions are related as follows:

$$\kappa_x(z) = \frac{1}{\gamma mv^2} k_x(z). \tag{37}$$

Lastly, we introduce the r.m.s. beam widths $\tilde{x}$ and $\tilde{y}$ for the x and y planes, respectively, as

$$\begin{aligned} \tilde{x} &\equiv \langle x^2 \rangle^{1/2}, \\ \tilde{y} &\equiv \langle y^2 \rangle^{1/2}. \end{aligned} \tag{38}$$

Note that we have $\langle x^2 \rangle'' = 2(\tilde{x}')^2 + 2\,\tilde{x}\,\tilde{x}''$ and $\langle y^2 \rangle'' = 2(\tilde{y}')^2 + 2\,\tilde{y}\,\tilde{y}''$.

Collecting these results and substituting them into Eq. (35) and its counterpart for the y direction yields the following set of equations for the r.m.s. beam envelopes:

$$\begin{aligned} \tilde{x}'' + \kappa_x(z)\tilde{x} - \frac{K}{2(\tilde{x}+\tilde{y})} - \frac{\tilde{\epsilon}_x^2}{\tilde{x}^3} - \frac{K}{b^4}(\tilde{x}^3 - \tilde{x}\tilde{y}^2) &= 0, \\ \tilde{y}'' + \kappa_y(z)\tilde{y} - \frac{K}{2(\tilde{x}+\tilde{y})} - \frac{\tilde{\epsilon}_y^2}{\tilde{y}^3} - \frac{K}{b^4}(\tilde{y}^3 - \tilde{y}\tilde{x}^2) &= 0, \end{aligned} \tag{39}$$

These equations are essentially the same as Sacherer's but with the addition of the image terms. From the above, we may write the equations for the equivalent KV beam with uniform charge density. Defining the envelopes of this equivalent beam in the x and y planes by $X(z)$ and $Y(z)$, respectively, we know that

$$\begin{aligned} X(z) &= 2\tilde{x}(z), \\ Y(z) &= 2\tilde{y}(z), \end{aligned} \tag{40}$$

for such a beam. Therefore, the equation governing the behavior of the equivalent KV beam for any distribution with elliptical symmetry is the following:

$$\begin{aligned} X'' + \kappa_x(z)X - \frac{2K}{X+Y} - \frac{\epsilon_x^2}{X^3} - \frac{K}{4b^4}(X^3 - XY^2) &= 0, \\ Y'' + \kappa_y(z)Y - \frac{2K}{X+Y} - \frac{\epsilon_y^2}{Y^3} - \frac{K}{4b^4}(Y^3 - YX^2) &= 0, \end{aligned} \tag{41}$$

where the quantities ϵ_x and ϵ_y are known as the effective emittances of the beam and are given by $4\tilde{\epsilon}_x$ and $4\tilde{\epsilon}_y$, respectively. These equations are recognized as the standard KV coupled-envelope equations with the addition of a term (for each equation) to account for the dominant image effects. Since the beam is centered and has elliptical symmetry, $\langle x^3 \rangle$ will be zero and the next image term will be an octupole term.

5.0 EXAMPLES AND ANALYSIS

We may use Eqs. (41) to explore the effects of the beam pipe on the beam dynamics. In this section we present three example situations to determine the significance of image effects in typical applications. The first example is a periodic transport channel made of (magnetic) quadrupole lenses. This example we treat completely analytically by comparing the relative strengths of the competing terms in Eqs. (41). The second example is the approximate analysis of a sheet beam in a cylindrical pipe. The third example is a matching section for a quadrupole transport channel used in the University of Maryland's Electron Ring Experiment[8,9]. In this example we numerically integrate Eqs. (41) for the matching section to analyze the effects of images.

5.1 Periodic Transport Channel

Consider a periodic transport channel made up of magnetic quadrupoles in a FODO arrangement (focusing, drift, defocusing, drift). Assume that we have a matched beam with equal x and y emittances. In addition assume that the FODO channel is symmetric, that is it has equal focusing and defocusing strengths in each plane. In such a periodic channel, the beam envelopes X and Y will oscillate 180 degrees out of phase with each other. We denote the minimum and maximum beam envelope excursions for these oscillations (for both planes) as X_{min} and X_{max}, respectively. Therefore, at some axial location X will be at a maximum (with value X_{max}) and Y will be at a minimum (with value X_{min}). This position will be the location of maximum image effects. It will be our goal to find the channel parameters which will keep the image forces below a given tolerance factor T

Since we are interested in space-charge dominated particle beams, we start by analyzing the ratio of the image term to the space-charge term (in such a beam $2K/(X+Y)$ will be the dominant self-term). To maintain our tolerance, this ratio must be less than the prescribed value T. At the axial location where image forces are maximal this ratio is

$$\frac{R}{4b^4} X_{\max}\left(X_{\max}^{\,2} - X_{\min}^{\,2}\right), \tag{42}$$

where R denotes the average radius of the beam; for the periodic channel we have $R=(X_{max}+X_{min})/2$. We may parameterize the maximum and minimum beam excursions by introducing the ripple parameter Δ. This parameter is defined as follows:

$$\begin{aligned} X_{\max} &= (1+\Delta)R, \\ X_{\min} &= (1-\Delta)R. \end{aligned} \tag{43}$$

Inserting these values into Eq. (42) yields

$$\frac{R^4}{b^4}(\Delta + \Delta^2). \tag{44}$$

Thus, to keep the image effects less than a factor T of the overall beam dynamics we must have

$$\frac{R}{b} < \left[\frac{T}{\Delta + \Delta^2}\right]^{1/4} . \qquad (45)$$

In order to get a flavor for this requirement we apply this formula to some typical numbers. If we pick a large but reasonable value for the ripple factor, say 0.3, we find that to maintain a tolerance factor of T=0.10 (10% tolerance) the ratio R/b must be less than 0.7, which means that X_{max} is less than $0.9b$. For T=0.05 (5% tolerance) we find that R should be less than $0.6b$ and X_{max} less than $0.8b$. Thus, these effects should be minimal in most situations. Only when the beam fills a substantial portion of the beam pipe and is sufficiently eccentric (continuous, round beams do not experience image effects) will images play a significant role.

For an emittance dominated beam we form the ratio between the image term and the emittance term. At our point of maximal X excursion we find this ratio to be

$$\frac{K}{\epsilon_x^2}\frac{R^6}{b^4}(1+\Delta)^4\Delta . \qquad (46)$$

We can simplify the analysis by realizing for the emittance-dominated beam the emittance term must be much greater than the perveance term. This requirement yields the inequality

$$\frac{\epsilon_x^2}{K} \gg R^2(1+\Delta)^3 . \qquad (47)$$

In order to satisfy the above, let us say that $\epsilon_x^2/K = GR^2(1+\Delta)^3$ where G is a large number. Then for a tolerance factor T we find from Eq. (46) that

$$\frac{R}{b} < \left[\frac{GT}{\Delta + \Delta^2}\right]^{1/4} . \qquad (48)$$

Comparing this equation to Eq. (45) we see that the image forces for an emittance-dominated beam can potentially be more significant because of the factor $G^{1/4}$.

5.2 Sheet Beam

We may use the results of Section 4 to approximate the image effects on a sheet beam in a cylindrical pipe. For such a beam we assume that the beam dimensions are much larger in one plane than in the other. The result is a beam which is fairly flat, or a sheet. These types of beams are used in free-electron lasers, for instance. We consider only the space-charge dominated regime. It will be our goal to determine the design parameters which maintain the image effects below a given tolerance T.

Without loss of generality we will assume that the x plane has the larger beam dimension. Therefore, the image effects will be at a maximum when X has a maximum, call this X_{max}, and Y has a minimum, call this Y_{min}. Let ν denote the ratio of X_{max} to Y_{min}, that is

$$\nu \equiv \frac{X_{max}}{Y_{min}} . \qquad (49)$$

Typically ν will have values of 5 or larger for sheet beams. We mention that the y plane emittance will be about ν times the x plane emittance due to beam compression. However, since we are only interested in the space-charge dominated situation we will not consider this effect. As before, we form the ratio of the image term to the space-charge term in Eq. (41) in order to analyze the effects of images. Again letting T denote the tolerance factor for the image effects, we have

$$\frac{1}{8b^4} X_{max}(X_{max}^2 - Y_{min}^2)(X_{max} + Y_{min}) < T, \tag{50}$$

for the x plane and

$$\left| \frac{1}{8b^4} Y_{min}(Y_{min}^2 - X_{max}^2)(Y_{min} + X_{max}) \right| < T, \tag{51}$$

for the y plane. Note that in this situation the image forces are defocusing in the x plane and focusing in the y plane (thus, the absolute value is necessary in Eq. (51)). Solving Eq. (49) for X_{min} then substituting into the above two equations yields

$$\frac{X_{max}}{b} < \left[\frac{8\nu^3}{\nu^3 + \nu^2 - \nu - 1} \right]^{1/4} T^{1/4}, \tag{52}$$

for the x plane and

$$\frac{X_{max}}{b} < \left[\frac{8\nu^4}{\nu^3 + \nu^2 - \nu - 1} \right]^{1/4} T^{1/4}, \tag{53}$$

for the y plane. Since ν is always greater than 1, the y plane's requirement is automatically satisfied whenever the x plane's tolerance is met. Thus, we need only consider Eq. (52).

We may rewrite Eq. (52) as

$$\frac{X_{max}}{b} < P(\nu) T^{1/4}, \tag{54}$$

where $P(\nu)$ is the function defined by

$$P(\nu) \equiv \left[\frac{8\nu^3}{\nu^3 + \nu^2 - \nu - 1} \right]^{1/4}. \tag{55}$$

The function $P(\nu)$ is plotted in Fig. 3. It blows up at the point ν=1 (since there are no image effects for a round beam) then asymptotically approaches $8^{1/4}$ as ν approaches infinity. Note, however, that at ν=3 there is an absolute minimum of P(ν) in the interval $[1,\infty)$. This indicates a resonance condition in the beam pipe. Therefore, to maintain the safest possible margin, the ratio X_{max} to b should always be kept below the value $P(3)T^{1/4}=(27/4)^{1/4}T^{1/4}\approx 1.612T^{1/4}$. For the tolerances of T=0.05 (5%) and T=0.10 (10%) this would require $X_{max}<0.762b$ and $X_{max}<0.906b$, respectively.

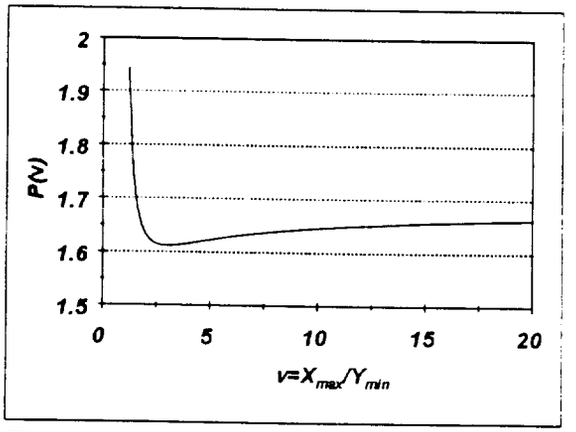

Figure 3: Image effect tolerance function for a sheet beam.

To get an appreciation for the full condition, consider the case where ν=5 and we want a 10% tolerance (T=0.1). We find that X_{max} must be less than $0.92b$. This condition should be fairly easy to meet in order to ignore image effects. For the more demanding case of ν=10 and a 5% tolerance (T=0.05) we must have $X_{max}<0.78b$ in order to avoid significant effects from images. Obviously in this situation the designer must be much more conscience of the role of images. Finally, we note that as ν becomes large, say greater than 10, the tolerance condition approaches $X_{max}<8^{1/4}T^{1/4}b$ and is essentially independent of the ratio ν. To compare this situation with the safest tolerance margin (evaluating P at ν=3) consider the tolerances of T=0.05 and T=0.10. This requires $X_{max}<0.795b$ and $X_{max}<0.946b$, respectively.

6.3 Quadrupole Matching Section

In the University of Maryland's Electron Ring Experiment a matching section of five lenses is used to match an electron beam from its cathode source to a transport channel composed of magnetic quadrupole lenses. The matching section is composed of one (initial) solenoid lens followed by four magnetic quadrupole lenses. The quadrupole lenses are arranged so that they have the same axial locations as the lenses in the transport channel, but their focusing strengths remain independent. Figure 4a shows the simulation results for the matching section obtained by a fourth-order Runge-Kutta integration of Eqs. (41). In this figure, both the X and Y envelopes of the beam are shown with and without image effects from a beam pipe with radius b=1.5cm. The solid lines represents the free-space solution while the dashed lines show the solution with image effects from the pipe. Figure 4b shows the focusing function $\kappa_x(z)$ for the matching section. Since the first lens is a solenoid it is focusing in both planes, the X and Y envelopes do not separate until the beam passes through the second lens.

One can see that the image effects do not play a large role in the beam dynamics. However, one can also see that the beam will no longer be matched to the transport channel, so it is not an insignificant effect in this situation. Matching sections, in general, will probably be more susceptible to image effects since the beam envelopes tend to make larger excursions through them. In this example we did not see an appreciable effect until the beam pipe radius was decreased to

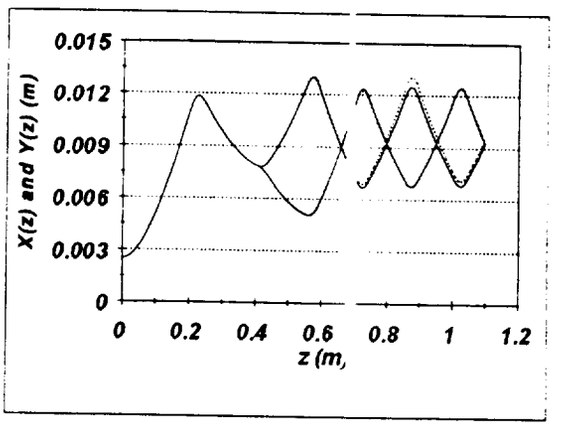

a)

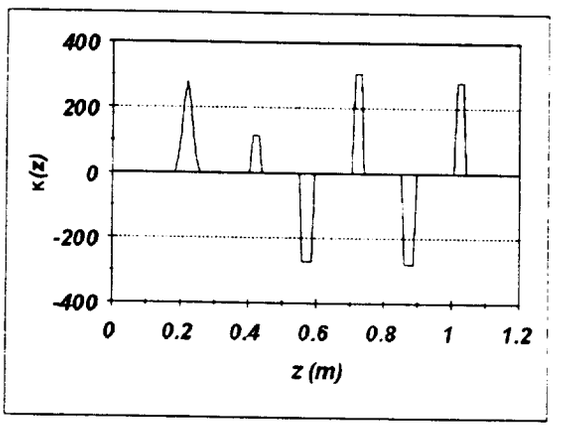

b)

Figure 4: Image effects for a magnetic quadrupole matching system.

1.5cm. Notice that the images affect the beam most around the axial location z=0.6m, where the difference in the X and Y envelopes is at a maximum and the beam's Y envelope fills 87% of the pipe. At this point the Y envelope experiences a slight defocusing due to the pipe and subsequently remains slightly larger than its free-space trajectory.

6.0 CONCLUSION

We have found that under certain circumstances image effects play a significant role in the dynamics of continuous beams having elliptical symmetry. When the beam is sufficiently eccentric and fills out a substantial portion of the beam pipe the image forces will notably affect the beam dynamics. In practice, these situations will most likely occur in matching sections where the beam experiences large eccentricities and large excursions through the beam pipe. In circumstances where the beam envelope excursions in the two transverse planes are less extreme, that is they do not deviate much from the average radius, we expect the image forces considered here to be insignificant. In these situations perhaps a more important effect from images would be due an off-centered beam. In this case the image forces would draw the entire beam farther away from its center position. This effect is widely known and is covered in Ref. 9, Chapt. 4.

As mentioned previously this approach is not self-consistent, unless we are fortunate enough to know the values of the r.m.s. emittances along the channel. Since the image effects are nonlinear, the r.m.s. emittances will typically increase through the channel, which violates the assumption of constant emittances. However, for space-charge dominated situations the increased emittance is a minor effect. Thus, our model will still yield meaningful results. More importantly, we have a way to not only simulate the beam dynamics with images but also to analytically quantify when these effects will play a significant role. It would seem that the best design strategy is to avoid such effects. The work presented in this paper will provide the designer with an easy way to check that his or her design will minimize any unwanted influences from image forces.

ACKNOWLEDGMENTS

The authors wish to thank Richard Cooper for many useful suggestions and corrections in preparing this manuscript.

Appendix A: Reduction of the Free-Space Component of $\langle xE_x \rangle$

We use the convergent geometric series to reduce the infinite summations in Eq. (29) to closed form. Recall that the geometric series has the property

$$\sum_{n=0}^{\infty} \alpha^n = \frac{1}{1-\alpha}, \tag{56}$$

where α is complex with $|\alpha|<1$. If we decompose the cosine function into its Euler exponents and employ the above formula we find

$$\sum_{n=1}^{\infty} \frac{r_s^{\,n}}{r^n} \cos n(\theta - \theta_s) = \frac{1}{2} \sum_{n=0}^{\infty} \left[\frac{r_s}{r} e^{i(\theta - \theta_s)} \right]^n + \frac{1}{2} \sum_{n=0}^{\infty} \left[\frac{r_s}{r} e^{-i(\theta - \theta_s)} \right]^n - 1,$$

$$= \frac{r^2 - r r_s \cos(\theta - \theta_s)}{r^2 + r_s^{\,2} - 2 r r_s \cos(\theta - \theta_s)} - 1. \tag{57}$$

Likewise for the sine function we get

$$\sum_{n=1}^{\infty} \frac{r_s^{\,n}}{r^n} \sin n(\theta - \theta_s) = \frac{1}{2i} \sum_{n=0}^{\infty} \left[\frac{r_s}{r} e^{i(\theta - \theta_s)} \right]^n - \frac{1}{2i} \sum_{n=0}^{\infty} \left[\frac{r_s}{r} e^{-i(\theta - \theta_s)} \right]^n,$$

$$= \frac{r r_s \sin(\theta - \theta_s)}{r^2 + r_s^{\,2} - 2 r r_s \cos(\theta - \theta_s)}. \tag{58}$$

Using the above two expressions and the trigonometric identities

$$\begin{aligned} &-2 \sin\theta_s \cos\theta_s \sin(\theta - \theta_s) \\ &= \left[\cos^2\theta - \cos^2\theta_s\right] \cos(\theta - \theta_s) + \left[\sin\theta\cos\theta - \sin\theta_s \cos\theta_s\right] \sin(\theta - \theta_s), \end{aligned} \tag{59}$$

and

$$\cos\theta\cos\theta_s = \cos^2\theta_s \cos(\theta - \theta_s) - \sin\theta_s \cos\theta_s \sin(\theta - \theta_s), \tag{60}$$

we can reduce Eq. (29) to Eq. (30).

Appendix B: Moments in Polar Coordinates

The first four moments of distribution $n(r, \theta) = f\left[r^2 u(\theta)\right]$ are readily computed as

$$\begin{aligned} \langle 1 \rangle &= \frac{1}{2N} \int_0^{2\pi} \frac{1}{u(\theta)} d\theta \int_0^{\infty} f(s)\, ds = \frac{\pi a_x a_y}{N} \int_0^{\infty} f(s)\, ds, \\ \langle x \rangle &= \frac{1}{2N} \int_0^{2\pi} \frac{\cos\theta}{u^{3/2}(\theta)} d\theta \int_0^{\infty} s^{1/2} f(s)\, ds = 0, \\ \langle x^2 \rangle &= \frac{1}{2N} \int_0^{2\pi} \frac{\cos^2\theta}{u^2(\theta)} d\theta \int_0^{\infty} s f(s)\, ds = \frac{\pi a_x^{\,3} a_y}{2N} \int_0^{\infty} s f(s)\, ds, \\ \langle x^3 \rangle &= \frac{1}{2N} \int_0^{2\pi} \frac{\cos^3\theta}{u^{5/2}(\theta)} d\theta \int_0^{\infty} s f(s)\, ds = 0, \end{aligned} \tag{61}$$

where the integrations are separated with the substitution $s = r^2 u(\theta)$. The values for y moments are obtained by substituting the sine function for the cosine function in the above. These equations are

also valid for a distribution in a beam pipe with radius b as long as we assume that f and b are such that $f[b^2u(\theta)]=0$ for all θ in $[0,2\pi]$. In other words, the beam does not touch the pipe.

REFERENCES

[1] C.K. Allen, N. Brown, and M. Reiser, "Image Effects for Bunched Beams in Axisymmetric Systems", *Particle Accel.*, Vol. **45** (1994), pp. 149-165.

[2] C.K. Allen and M. Reiser, "Zero-Temperature Equilibrium for Bunched Beams in Axisymmetric Systems", *Particle Accel.*, Vol. **48** (1995), pp. 193-211.

[3] F.R. Sacherer, "RMS Envelope Equations with Space Charge", *IEEE Trans. Nucl. Sci.* **NS-18** (1971), pp. 1105-1107.

[4] I.M. Kapchinskij and V V Vladimirskij, Proc. Int. Conf. on High-Energy Accelerators and Instrumentation, CERN 1959, pp. 274-288.

[5] D.D Holm, W P Lysenko, and J.C. Scovel, "Moment Invariants for the Vlasov Equation", *J. Math. Phys.*, Vol. **31**, No. 7 (July 1990), pp. 1610-1615.

[6] I. Stakgold, *Green's Functions and Boundary Value Problems* (Wiley, NY, 1979), pp. 506. The Green's function for the case $b=1$ is derived. The analysis is easily generalized for the cases $b \neq 1$.

[7] M. Reiser, *Theory and Design of Charged Particle Beams* (Wiley, 1994), pp. 197, 257.

[8] M. Reiser, S. Bernal, A. Dragt, M. Venturini, J.G. Wang, H. Onishi, and T.F. Godlove, "Design Features of a Small Electron Ring for Study of Recirculating Space-Charge Dominated Beams", (submitted to *Fusion Energy and Design*).

[9] S. Bernal, A. Dragt, M. Reiser, M. Venturini, and J.G. Wang, "Matching Section and Injector Design for a Model Electron Ring", 1995 HIF Symp., Princeton (to be published).